Research on the Electromagnetic Emission Along the Contact Line of Electrified Trains Passing Through Neutral Sections

Liu Guang-hui, Wang Yapeng, and Li Zhenghui

School of Electrical Engineering
Zhengzhou Railway Vocational and Technical College, Zhengzhou, Henan, 451460, China
liuguanghui@zzrvtc.edu.cn

Abstract – To study the electromagnetic emission along a contact line when an electrified high-speed train passes through a neutral section, this paper models the transmission line of the traction network, provides a calculation method and boundary conditions for the parameters of the model, solves for the current distribution along the contact line, and calculates the electromagnetic emission of the contact line considering the antenna effect. Thus, the electromagnetic emission characteristics along the electrified railway are determined. Moreover, the actual electromagnetic emissions of a train passing through a neutral section are measured with a field test method and compared with the calculation results to verify the effectiveness of the model.

Index Terms – electrified high-speed railway, electromagnetic emission, electromagnetic environment test, transmission line theory.

I. INTRODUCTION

With the rapid development of transportation, science and technology, many cities in China have begun to build comprehensive transportation systems. Electrified high-speed railways (HSRs) in airports will become one of the future trends of integrated transportation. However, due to the existence of offline arcs, electrified high-speed trains generate high-frequency and broadband electromagnetic interference during operation [1–3]. Due to the mechanical vibration of the pantograph, an offline arc will be generated, which will generate high-frequency current components and radiation to the outside world. Especially when a train passes through the neutral section, it will inevitably produce an offline arc and a large number of electromagnetic emissions [4–5]. At present, many studies have been carried out on the mechanism behind the offline arc between a pantograph and a catenary [6–7], with a large number of simulation models having been developed [8–9].

In fact, the electromagnetic emissions of electrified railways include not only the offline arc of the pantograph and catenary but also that of the contact line. As early as 2001, researchers found that electromag-netic emission of the traction network is the result of the offline arc, the electromagnetic emission efficiency of the overhead line in the traction network is much higher than the offline arc of the pantograph and catenary [10]; however, this discovery has not attracted much attention. In this paper, by modeling the catenary of an electrified high-speed train, the current distribution and electromagnetic emission of the catenary are calculated to support the electromagnetic compatibility in electrified railways.

II. NEUTRAL SECTION ARRANGEMENT

As shown in Fig. 1, the public grid supplies energy for the overhead contact system (OCS), which is three-phase, despite the OCS adopting a single phase [11–12]. The external power source uses a traction substation to step down the voltage and convert three-phase AC to single-phase AC. To balance the load of the A, B and C phases of the public power system, it is generally required to implement an A and B (or A and C or B and C) phase alternating power supply. In this implementation, A and B must be separated from each other because their phases are different. Therefore, phase separation devices must be installed at the outlet of a traction substation and between two traction substations (feeding section ends).

As shown in Fig. 2, and as determined by the different running speeds of locomotives, insulated overlap or neutral insulators can be used as neutral sections [13–14]. Insulated overlaps rely on air for insulation, while
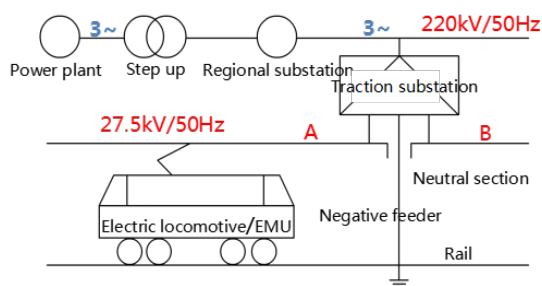

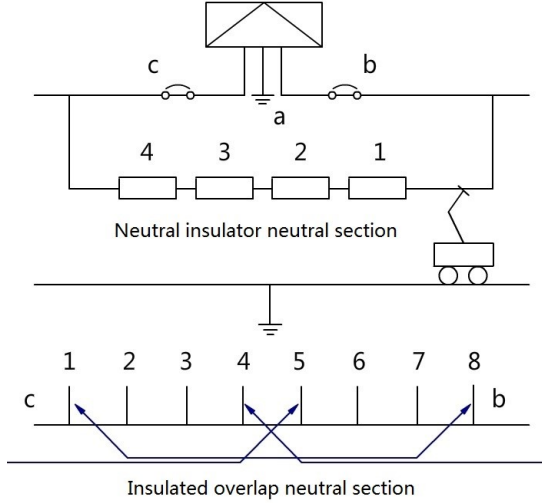Fig. 1. Diagram of catenary power supply.

Fig. 2. Classification of neutral section.

neutral insulators rely on solid- and gas-based insulation. No matter the type of neutral section, pantograph arcing will be generated when the train passes through it.

III. TRACTION NETWORK ELECTROMAGNETIC EMISSION MODEL

When electrified trains run normally, the pantograph of the train contacts a contact wire, and the traction network supplies power through this contact line. Due to the mechanical vibration of the train during its normal driving, the pantograph and contact line will be briefly separated, and an offline gap will appear between the two lines, resulting in arc discharges between the contact wire and pantograph, as shown in Fig. 3.
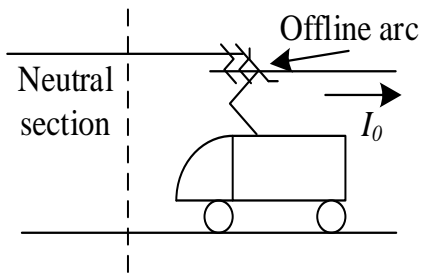

Fig. 3. Overhead contact wire model.

Many studies show that offline arcs produce conduction current excitation on a line, such that the contact line produces an external electromagnetic emission. This contact wire-destructive earth transmission line model is shown in Fig. 4. This model for the overhead line can effectively calculate the electromagnetic emission on the contact line.
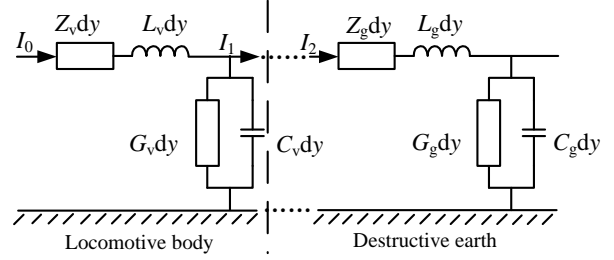

Fig. 4. Overhead line model equivalent circuit.

The model is divided into two circuits, the contact line-locomotive body circuit and the contact line-damaged earth circuit, as shown in Fig. 4. Because the contact line is a good conductor, its small impedance can be ignored, and only the locomotive body and damaged earth impedances are considered. In the model, Z_v and Z_g are the unit length impedances of the car body and damaged earth, L_v and L_g are the unit length inductances of the car body and damaged earth, C_v and C_g are the unit length capacitances of the car body and damaged earth, G_v and G_g are the unit length conductances of the car body and damaged earth, and I_0 is the initial current. Among these values, the wire impedance is [15]:

$$Z_l = \frac{1}{2r}\sqrt{\frac{\mu_l f}{\pi \sigma_l}}, \qquad (1)$$

where r is the contact wire radius, σ_l is the conductor conductivity, μ_l is the conductor magnetic permeability, and f is the frequency. The locomotive body impedance is [15]:

$$Z_v = \frac{1}{4\pi r}\sqrt{\frac{\mu_v}{\pi \sigma_v f}}, \qquad (2)$$

where σ_v is the locomotive body conductivity, μ_v is the car body magnetic permeability. The damaged earth impedance is [16]:

$$Z_g = \frac{j\omega\mu_0}{2\pi}\ln\frac{1+\gamma_g h}{\gamma_g h}, \qquad (3)$$

where μ_0 is the vacuum permeability, h is the height between the contact line and the ground, $\omega = 2\pi f$, f is the frequency, and γ_g is the earth propagation coefficient, which can be written as [16]:

$$\gamma_g = \sqrt{j\omega\mu_0(\sigma_g + j\omega\varepsilon_g)}. \qquad (4)$$

The system's inductance L and capacitance C can be expressed as [16]:

$$L = \frac{\mu_0}{2\pi}\ln\frac{2h}{r}, \qquad (5)$$

$$C = \frac{2\pi\varepsilon_0}{\ln(2h/r)}, \qquad (6)$$

where r is the radius of the wire. It is possible to obtain the contact line-car body circuit inductance L_v and capacitance C_v, and the contact line-damaged earth circuit inductance L_g and capacitance C_g. Since

there is no conducting current between the contact line and the damaged earth, G can be ignored.

The telegraph equation for the transmission line model shown in Fig. 4 can be written as [17]:

$$\frac{dU(y)}{dy} + ZI(y) = 0, \tag{7}$$

$$\frac{dI(y)}{dy} + YU(y) = 0, \tag{8}$$

and in the formulae:

$$Z = (Z_l + Z_g + L), \tag{9}$$

$$Y = \frac{1}{j\omega C}, \tag{10}$$

where the boundary condition of the model at the initial position is I_0, and the terminal is the other end of the power supply zone (the traction transformer), which can be set as an open circuit with boundary condition written as:

$$I_{a1}(y = 0) = I_0, \tag{11}$$

$$I_{a1}(y = l_v) = I_{a2}(y = l_v), \tag{12}$$

$$I_{a2}(y = l_a) = 0, \tag{13}$$

where l_v is the car body length of the contact line-car body circuit, and l_a is the entire model length (the length of the power supply zone). A general solution is obtained from equation (7) and equation (8), equations (11)–(13) are boundary conditions, so the current distribution on the contact line can be solved as follows:

$$\begin{bmatrix} 1 & -1 & 0 & 0 \\ e^{-\gamma_1 l_v} & -e^{\gamma_1 l_v} & -e^{\gamma_2 l_v} & e^{\gamma_2 l_v} \\ Z_{01}e^{-\gamma_1 l_v} & Z_{01}e^{\gamma_1 l_v} & -Z_{02}e^{-\gamma_2 l_v} & -Z_{02}e^{\gamma_2 l_v} \\ 0 & 0 & e^{-\gamma_2 l_a} & -e^{\gamma_2 l_a} \end{bmatrix} \begin{bmatrix} I_{a1}^+ \\ I_{a1}^- \\ I_{a2}^+ \\ I_{a2}^- \end{bmatrix}$$
$$= \begin{bmatrix} I_0 \\ 0 \\ 0 \\ 0 \end{bmatrix}, \tag{14}$$

where γ_0 is the propagation coefficient, and Z_0 is the characteristic impedance, which can be written as [17]:

$$\gamma_0 = \sqrt{ZY}, \tag{15}$$

$$Z_0 = \sqrt{Z/Y}, \tag{16}$$

where the reflux conductors below the overhead line are different, and their corresponding impedances Z and conductors Y vary. To find the initial current I_0, a modified Habedank model [18] is used with a mathematical expression as follows:

$$\begin{cases} \frac{dg_C}{dt} = \frac{1}{\tau_0 g_H{}^n}\left(\frac{i^2}{u^2 g_C} - g_C\right) \\ \frac{dg_M}{dt} = \frac{1}{\tau_0 g_H{}^n}\left(\frac{i^2}{kg^\beta d_{max}} - g_M\right) , \\ g_H = \frac{1}{g_C} + \frac{1}{g_M} \end{cases} \tag{17}$$

where, i is the arc current, g_C is the Cassie arc model instantaneous conductance, g_M is the Mayr arc model instantaneous conductance, g_H is the instantaneous conductance of the Habedank arc model, n is a constant, τ_0 is the initial time constant, u is the Habedank arc model

voltage gradient, β and k represent the power factor and dielectric coefficient of dissipation power, respectively, and d_{max} represents the maximum distance between the pantograph and contact wire.

According to the current distribution along the contact line, the electromagnetic emission can be calculated using the antenna effect. This calculation of electromagnetic emission is shown in Fig. 5. Because the calculation frequency is less than 30 MHz, the magnetic field strength is calculated directly [16]:

$$dH = \frac{I(y)dy}{4\pi r^2} e^{-j\frac{2\pi r}{\lambda}}\left(1 + j\frac{2\pi r}{\lambda}\right)\sin\theta. \tag{18}$$
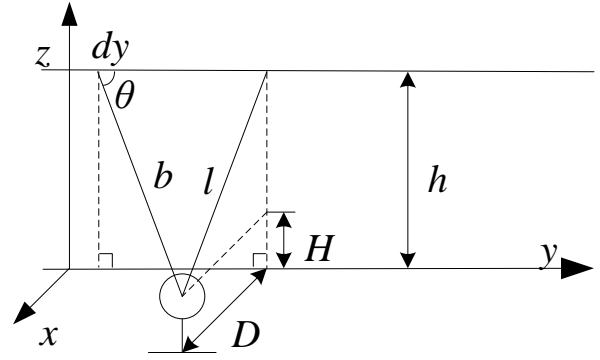

Fig. 5. Model for electromagnetic emission.

The equation's geometric relationship is shown in Fig. 5. Since the calculation frequency is less than 30 MHz and the distance r from the antenna to the contact line is much less than the calculated wavelength λ, equation (18) can be reduced according to near-field conditions $r \ll \lambda$:

$$dH = \frac{I(y)dy\sin\theta}{4\pi r^2}, \tag{19}$$

where:

$$r = \sqrt{D^2 + l^2 + y^2}, \tag{20}$$

$$\sin\theta = \frac{l}{b}. \tag{21}$$

Subsequently, dH is integrated in segments of the entire power supply zone, the contact line-locomotive body circuit is integrated, and the contact line-damaged earth circuit is integrated to obtain the total electromagnetic emission value:

$$\begin{aligned} H &= \int_0^{l_v} dH + \int_{l_v}^{l_a} dH \\ &= \frac{l}{4\pi r^2}\Big[\int_0^{l_v} \frac{I(y)}{\sqrt{D^2 + l^2 + y^2}}dy \\ &\quad + \int_{l_v}^{l_a} \frac{I(y)}{\sqrt{D^2 + l^2 + y^2}}dy\Big], \end{aligned}$$

$$\tag{22}$$

Table 1: Used parameters

Symbol	Parameter	Symbol	Parameter
r	0.00645 m	μ_0	$4\pi \times 10^{-7}$ H/m
σ_l	5.8×10^7 S/m	ε_0	8.85×10^{-12} F/m
σ_v	2×10^7 S/m	σ_g	0.0001 S/m
μ_l	$4\pi \times 10^{-7}$ H/m	h_g	6.4 m
μ_v	1.75×10^{-7} H/m	h_v	2.4 m
D	10 m		

where $I(y)$ is the current distribution on the feeding section as calculated by equation (14). The specific calculated parameters are shown in Table 1.

IV. TRACTION NETWORK ELECTROMAGNETIC TRANSMISSION TEST

According to GB/T24338.2 [19], an EMI R&S test receiver is used from 9 kHz to 3 GHz to test the magnetic field intensity. An R&S ring antenna HFH2-Z2 is used to receive the magnetic field from 8.3 kHz to 30 MHz, and a high-frequency cable is used between them. The test position is on the field side of an electrified railway track, and electromagnetic emission values are recorded when the train is coming and without any trains (background). The test parameters are set in strict accordance with GB/T24338.2. The test instrument, test antenna, test site and test layout are shown in Fig. 6.

In Fig. 6 (d), TP represents a test point, which is the position of a receiving antenna. Test point TP_1 is used to record the electromagnetic field value when the train passes through the neutral section. Test points TP_2 and TP_3 verify the distribution of these electromagnetic emissions along the railway. Variables d_1 and d_2 are the distances between the test point and neutral section, with d_1 being 600 m and d_2 being 800 m. The test data are shown in Table 2. The values represent electromagnetic emission data tested when the vehicle passed through the neutral section, and the background values represent data tested when no locomotive passed through.

During experimentation, an electromagnetic environment test instrument is installed at a vertical distance of 10 m from the electrified railway. First, an EMI receiver is installed and connected to a 220 V power source. Second, a HFH2-Z2 ring antenna is installed with the ring plane parallel to the electrified railway. Finally, a receiver is connected to the ring antenna with a high-frequency shielding cable. These test parameters were set according to GB/T 24338-2. When no electrified trains pass, a background electromagnetic environment test is conducted, and these test data are background data. When an electrified train is coming, interference and electromagnetic tests are conducted. The
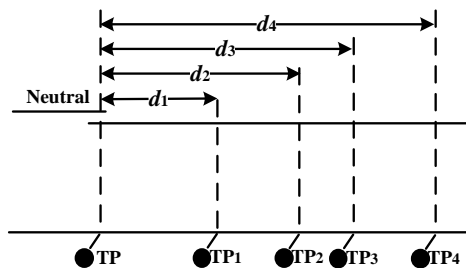

(a) EMI R&S receiver

(b) Ring antenna

(c) Test field

(d) Arrangement for testing

Fig. 6. Test diagram.

data obtained from these tests characterize the electromagnetic emission profiles of electrified railways when a train passes through a neutral section.

As Table 2 shows, the very stable background data are generally maintained at approximately 26 dBμA/m. The signal when a train passes through the neutral section is larger than the background signal by 40 dB to 55 dB. Since the TP is located in the neutral section, its electromagnetic emission value is the maximum

Table 2: Test data

Test Point	Background (dBµA/m)	Train Incoming (dBµA/m)
TP	27.23	81.97
TP_1	25.56	78.15
TP_2	25.12	68.67
TP_3	26.92	64.45
TP_4	26.54	54.13

and reaches 81.97 dBµA/m. The TP_1, TP_2, TP_3 and TP_4 are located along the electrified railways at 400 m, 600 m, 800 m and 1000 m away from the neutral section, respectively. Their electromagnetic emission values are smaller than that of TP, at 78.15 dBµA/m, 68.67 dBµA/m, 64.45 dBµA/m and 54.13 dBµA/m.

V. COMPARISON OF RESULTS

As Fig. 3 shows, when a train is traveling from a feeding section to the neutral section, the current distribution on the contact line can be obtained by equation (14), as shown in Fig. 7. The current distribution of the overhead line-locomotive body circuit is depicted on the left side of the dotted line. The current distribution of the overhead line-damaged earth circuit is on the right side of the dotted line. Because the locomotive body conductivity is close to that of metal, it is a good conductor.

Given the locomotive body length, the medium frequency current in the contact line is an undamped oscillation. Moreover, the current oscillation is just cyclic, and the shock amplitude appears as two peaks, which are both 2.73 mA. This shock amplitude change is the same as that of the 1 MHz sine wave amplitude oscillation.

Due to much lossy grounding impedance, the current distribution on the model decayed significantly with axial distance by approximately 0.3 mA per 100 m. Around 1500 m from the neutral section, the current distribution on the wire attenuates to 1% of the peak value, which leads to the inference that strong electromagnetic emission appears on the overhead line at the beginning of the model.

After the current distribution on the contact line is obtained, the electromagnetic emission on the line can be obtained by equation (22). This is compared to the measured data, as shown in Fig. 8.

In Fig. 8, the blue curve shows the calculation of electromagnetic emission using the above transmission line model. The red star is the electromagnetic emission value recorded by TP_2, the green star is the electromagnetic emission value recorded by TP_3, and the black curve is the maximum value of the background data. As Fig. 8 shows, when an electric locomotive passes through the neutral section, the electromagnetic emission on the contact wire attenuates by approximately 10 dB every 200 m.
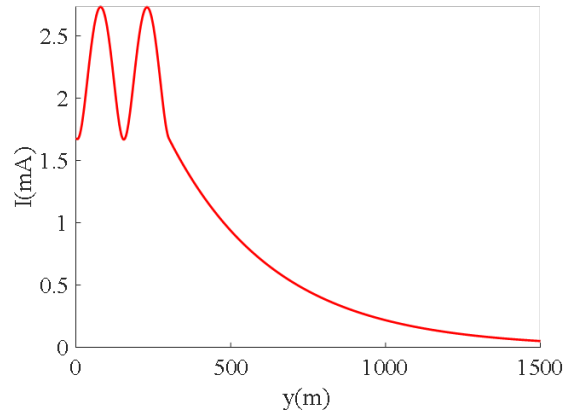

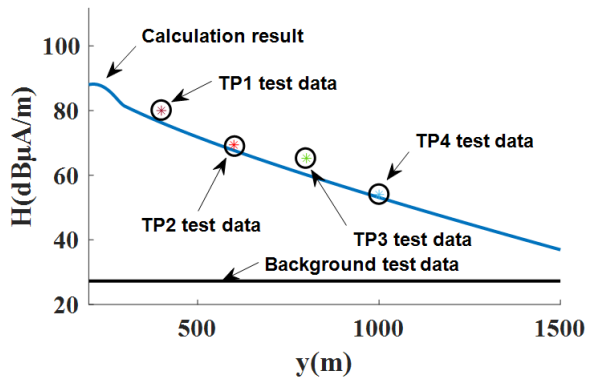Fig. 7. Contact line current distribution curve.

Fig. 8. Electromagnetic emission curve of the contact wire.

The calculation results agree with the measured values, which verifies the effectiveness of the model. If the distance between the neutral section and the measuring point is less than nearly 1500 m, the electromagnetic emission along the electrified railway gradually decays, from 88.16 dBµA/m to 36.95 dBµA/m. The closer to the neutral section, the greater the electromagnetic emission value is. The electromagnetic emission data measured at 600 m and 800 m from the neutral section agree with the calculation results, with differences within 3 dB. The calculation results and electromagnetic emission data are both greater than the background data, with the maximum data being 60.93 dB above the background test value. At 1500 m from the neutral section, its calculation results are 9.72 dB higher than the background data.

VI. CONCLUSION

Combined with GB/T24338.2, a model for electromagnetic emission on a contact wire is established to calculate the current distribution on the contact line, and

the antenna effect model is established for calculating the electromagnetic emission on the contact line. The electromagnetic emission characteristics on the contact wire are presented, and the electromagnetic emission mechanism is analyzed. The electromagnetic emission on the contact line changes linearly for damaged ground, which imparts an obvious attenuation of approximately 10 dB per 200 meters, and its value is approximately 88 dBμA/m at the first end.

As the distance from the neutral section increases, the electromagnetic emission value along the railway decreases to 36.95 dBμA/m at 1500 m. The electromagnetic emission data tested at 600 m and 800 m from neutral agreed with the calculation results. The model discrepancies are less than 3 dB, and the models provide values greater than the background data, proving the effectiveness of this transmission line modeling method. Using the model to research electromagnetic emissions along electrified railways, the calculation results are accurate and match the measured data. This study gives the electromagnetic emission value for a feeding section when a train passes a neutral section, to provide theoretical support for the electromagnetic compatibility of electrified high-speed railways.

ACKNOWLEDGEMENTS

REFERENCES

[1] Y. Xiaojia, Z. Feng, and Q. Riqiang, "Radiation characteristics of pantograph-catenary arc and its influence on airport glide beacon," *Acta Aeronautica et Astronautica Sinica*, vol. 39, no. 1 pp. 253-260, 2018.

[2] Y. Jiabin, Z. Feng, and L. Jun, "Electromagnetic interference measurement and analysis of high-speed electric multiple units speed sensor," *Journal of Electronic Measurement and Instrumentation*, vol. 29, no. 3, pp. 433-438, 2015.

[3] Z. Feng, T. Yutao, and G. Chenxuan, "Mechanism and suppression of electromagnetic interference of pantograph-catenary arc to speed sensor of CRH380BL electric multiple unit," *China Railway Science*, vol. 37, no. 6, pp. 69-74, 2016.

[4] H. Lu, F. Zhu, and Q. Liu, "Suppression of cable overvoltage in a high-speed electric multiple units system," *IEEE Transactions on Electromagnetic Compatibility*, vol. 61, no. 2, pp. 361-371, 2019.

[5] L. Hede, Z. Feng, and L. Xin, "Shielding effectiveness of reinforced concrete toward electric arcs in pantograph-catenary systems of metro," *Chinese Journal of Radio Science*, vol. 31, no. 6, pp. 1209-1215, 2016.

[6] S. Midya, D. Bormann, and A. Larsson, "Understanding pantograph arcing in electrified railways - influence of various parameters," 2008 *IEEE International Symposium on Electromagnetic Compatibility*, Detroit, MI, USA, pp. 1-6, 2008.

[7] S. Midya, D. Bormann, and T. Schutte, "Pantograph arcing in electrified railways—mechanism and influence of various parameters—part II: with AC traction power supply," *IEEE Transactions on Power Delivery*, vol. 24, no. 4, pp. 1940-1950, 2009.

[8] Y. Wang, Z. Liu, and X. Mu, "An extended Habedank's equation-based EMTP model of pantograph arcing considering pantograph-catenary interactions and train speeds," *IEEE Transactions on Power Delivery*, vol. 31, no. 3, pp. 1186-1194, 2016.

[9] J. L. Guardado, S. G. Maximov, and E. Melgoza, "An improved arc model before current zero based on the combined Mayr and Cassie arc models," *IEEE Transactions on Power Delivery*, vol. 20, no. 1, pp. 138-142, 2005.

[10] B. Tellini, M. Macucci, and R. Giannetti, "Conducted and radiated interference measurements in the line-pantograph system," *IEEE Transactions on Instrumentation and Measurement*, vol. 50, no. 6, pp. 1661-1664, 2001.

[11] Y. Wang, Z. Liu, and X. Mu, "Research on electromagnetic transient process in articulated split-phase insulator of high-speed railway considering viaduct's electrical coupling," *International Transactions on Electrical Energy Systems*, vol. 27, no. 4, 2017.

[12] K. Huang, Z. Liu, and Y. Wang, "Analysis of optimal body grounding technology in case of electric multiple unit passing neutral section device," *Proceedings of the CSU-EPSA*, vol. 28, no. 5, pp. 1-8, 2016.

[13] L. Xin, "Pantograph arcing electromagnetic radiation model of high-speed train passing electric phase separation and its typical application analysis," Ph.D. dissertation, Southwest Jiaotong University, Chengdu, China, 2019.

[14] W. Ying, L. Zhigang, and M. Xiuqing, "Study on pantograph-catenary system temperature field of high-speed railway under off-line arc conditions," *Computer Simulation*, vol. 32, no. 7, pp. 154-159, 2015.

[15] L. Hongmin, Y. Zhiyong, and L. Wanyu, *Engineering Electromagnetic Compatibility*, Xi'an, China: Xidian University Press, pp. 160-162, 2010.

[16] F. M. Tesche, M. V. Ianoz, and T. Karlsson, *EMC Analysis Methods and Computational Models*, New York, NY, USA: Wiley, 1997.

[17] C. R. Paul, *Analysis of Multiconductor Transmission lines*, 2nd ed., New York, NY, USA: Wiley, 2009.

[18] W. Ying, "Studies on the heat distribution and current conduction of pantograph-catenary electric contact and their influence laws," Ph.D. dissertation, Southwest Jiaotong University, Chengdu, China, 2015.

[19] *Railway applications - Electromagnetic compatibility - Part 2: Emission of the whole railway system to the outside world*, GB/T 24338-2, Ministry of Railways, PRC, China Standards Press, Beijing, 2018.

Liu Guang-hui was born in Henan, China, in 1989. He received the B.E. degree in Electric Engineering from Xuchang University, Xuchang, China, in 2013, and the M.S. degree in Electric Engineering from Southwest Jiaotong University, Chengdu, China, in 2016. His research interests include railway power supply and EMC.

Wang Yapeng was born in Henan, China, in 1994. He received the master's degree in Electrical Engineering from East China Jiaotong University, Nanchang, China, in 2019. His current research focus is on traction power supply systems.

Li Zhenghui was born in Henan, China, in 1993. He received the B.Eng. and M.Eng. degrees in the field of fault diagnosis from Luoyang Institute of Science and Technology, China, and Hangzhou Dianzi University, China, in 2015 and 2018, respectively. His current research interests include machine learning, fault diagnosis and pattern recognition.